Variational Bias Correction of GNSS ZTD in the HARMONIE Modeling System

JANA SÁNCHEZ ARRIOLA

State Meteorological Agency, Santander, Spain

MAGNUS LINDSKOG

Swedish Meteorological and Hydrological Institute, Norrköping, Sweden

SIGURDUR THORSTEINSSON

Icelandic Meteorological Office, Reykjavík, Iceland

JELENA BOJAROVA

Norwegian Meteorological Institute, Oslo, Norway, and Swedish Meteorological and Hydrological Institute, Norrköping, Sweden

(Manuscript received 21 May 2015, in final form 29 January 2016)

ABSTRACT

To fill the gap in the observation system for humidity, the HIRLAM–ALADIN Research on Mesoscale Operational NWP in Euromed (HARMONIE) limited-area high-resolution kilometer-scale model has been prepared for assimilation of Global Navigation Satellite System (GNSS) zenith total delay (ZTD) observations. The observation-processing system includes data selection, bias correction, quality control, and a GNSS observation operator for data assimilation. A large part of the bias between observations and model equivalents comes from the relatively low model top used in the HARMONIE experiments. The functionality of the different observation-processing components was investigated in detail as was the overall performance of the GNSS ZTD data assimilation. This paper contains an extensive description of the GNSS ZTD observation-processing system and a comparison of a newly introduced variational bias correction for GNSS ZTD data with an alternative static bias correction, as well as a detailed analysis of the impact of GNSS ZTD data, both in terms of statistical evaluations over a longer period and in terms of individual case studies. Assimilation of the GNSS ZTD observations with a variational bias correction has improved the quality of short-range weather forecasts for the moisture-related parameters in particular, both in a statistical sense and in individual case studies. The paper also discusses further improvements in the HARMONIE variational data-assimilation system that are needed to fully utilize the potential of high-resolution GNSS ZTD observations.

1. Introduction

Data assimilation in numerical weather prediction (NWP) optimally combines observations with an atmospheric model to spread the observed quantities and to produce the best possible model initial state. It was early realized (Lorenz 1965) that forecast quality is strongly dependent on an accurate description of the initial state. For short-range forecasting at a kilometer scale it is important to utilize observations with high spatial and temporal resolution to initialize mesoscale phenomena such as convective storms and sea breezes. Fabry and Sun (2010) particularly have shown that an accurate description of the initial moisture field is important for short-range forecasts of clouds and precipitation.

The HIRLAM–ALADIN Research on Mesoscale Operational NWP in Euromed (HARMONIE) modeling system is a high-resolution limited-area NWP system that is specially targeted for convective-scale phenomena (the definitions of HIRLAM, ALADIN, and other common meteorology-related acronyms can be found

Corresponding author address: Jana Sánchez Arriola, AEMET, Calle Ricardo Lorenzo s/n, 39071 Santander Cantabria, Spain.
E-mail: jsancheza@aemet.es

DOI: 10.1175/JAMC-D-15-0137.1

online at http://www.ametsoc.org/PubsAcronymList). This system is currently running operationally at several national weather services in Europe. It is based on scientific codes jointly developed by the ALADIN and HIRLAM consortia in a common modeling environment. The main components of the HARMONIE system are surface data assimilation, upper-air data assimilation, and a nonhydrostatic forecast model with Applications of Research to Operations at Mesoscale (AROME) physics (Seity et al. 2011) for the atmosphere and the Surface Externalisée (SURFEX) prognostic scheme for surface processes (Masson et al. 2013). In our experiments we used a horizontal resolution of 2.5 km and 65 vertical model levels. This configuration, denoted HARMONIE AROME 2.5, is targeted on an adequate description of the convective-scale phenomena and uses the six lowest model levels to describe the lowest 200 m of the atmosphere and a total of 15 model levels to describe the lowest 1000 m of the atmosphere. The HARMONIE AROME 2.5 model configuration is designed to have a very low model top: 10 hPa, which approximately corresponds to a 32-km height in the atmosphere. Several practical constraints and considerations were taken into account for this setup, among them being the computational efficiency and numerical stability of the system. As host-model information, operational forecasts from the European Centre for Medium-Range Weather Forecasts (ECMWF) are used. The surface data assimilation uses an optimal interpolation scheme (Giard and Bazile 2000). In the current study we used, for the upper air, a three-dimensional variational data-assimilation (3D-Var) scheme (Fischer et al. 2005) with a 3-h update cycle and climatological background-error statistics (Berre 2000). The only direct humidity measurements were provided by vertical profile measurements from radiosondes and by 2-m relative humidity measurements from surface synoptic (SYNOP) stations. The mesoscale atmospheric distribution of moisture in general was therefore not captured well because of this lack of humidity information.

The rapid development of moisture-related observations derived from the Global Navigation Satellite System (GNSS) has supplied a new source of mesoscale atmospheric humidity information. These data measure the delays in the receipt of the signal from the GNSS satellites by stations caused by the presence of neutral atmosphere and are expressed as excess pathlengths (Bevis et al. 1992). The ''EUMETNET'' GPS Water Vapor Program (E-GVAP) is a collaborative effort between the European geodetic community and several European national meteorological institutes. The purpose of E-GVAP is to provide atmospheric water vapor observations for use in operational meteorology. Zenith total delay (ZTD) observations obtained from the E-GVAP network of ground-based GNSS receivers contain horizontally dense information on the total columnar amount of water vapor. These observations are furthermore available with a temporal resolution of up to 15 min, and therefore they have the potential to fill in the lack of humidity data for kilometer-scale short-range weather forecasting.

A number of assimilation studies have shown a positive impact of GNSS ZTD observations on NWP systems at a horizontal model grid resolution on the order of 10 km (De Pondeca and Zou 2001; Vedel and Huang 2004; Cucurull et al. 2004; Poli et al. 2007; Macpherson et al. 2008; Yan et al. 2009a,b; Boniface et al. 2009; Benjamin et al. 2010; Shoji et al. 2011; Bennitt and Jupp 2012; Desroziers et al. 2012). The importance of combining the GNSS data with other types of observations has been highlighted in several studies (Cucurull et al. 2004; Desroziers et al. 2012; Sánchez-Arriola and Navascués 2007; Sánchez-Arriola et al. 2006). Some first encouraging results from assimilation of these observations at a kilometer-scale horizontal resolution have been obtained (Seity et al. 2011; de Haan 2013). To stimulate further enhancements of the use of GNSS ZTD observations in NWP—in particular, forecasts of severe weather in NWP and nowcasting applications—a new European Cooperation in Science and Technology (COST) Action (ES1206) has been initiated.

All types of measurements are associated with errors that need to be properly characterized within the data assimilation. Variational bias correction (Dee 2005) has proven successful in accounting for observation biases, but so far such correction has mainly been applied to various types of satellites (Auligne et al. 2007; Dee and Uppala 2009), although there are some recent developments toward other observation types, such as radiosonde measurements (Bosilovich et al. 2012) as one example. The difficulties of spatially and temporally correlated observation errors have generally been circumvented in data assimilation by applying thinning of data or through observation-processing algorithms that are assumed to remove the observation-error correlations (Stewart et al. 2013). Methods have been developed to account for serially correlated errors (Järvinen et al. 1999), but there is certainly room for improvement with regard to spatially correlated errors, although some general research within this area has been carried out (Lin et al. 2000; Liu and Rabier 2002; Stewart et al. 2013). Some studies have focused on GNSS ZTD observations (Kleijer 2001; Stoew 2004; Eresmaa and Järvinen 2005), but the treatment of correlated observation errors on the kilometer scale still remains a pioneering topic of research.

The HARMONIE AROME 2.5 model configuration has been prepared for assimilation of GNSS ZTD observations. The observation-processing system includes data selection, quality control, and bias correction. We employed a variational bias-correction device to handle systematic discrepancies between model equivalents and observed values. A large part of the systematic discrepancies was due to the low model top (10 hPa) applied in the HARMONIE AROME 2.5 configuration. The functionality of the different observation-processing components has been investigated in detail as was the overall performance of the GNSS data assimilation. This paper contains an extensive description of the observation-processing system and a comparison of a newly introduced variational bias correction for GNSS data with an alternative static bias correction, as well as a detailed analysis of the impact of GNSS data, both in terms of statistical evaluations over a longer period and in terms of individual case studies.

This paper is organized as follows: The observation-processing system is the topic of section 2. In section 3, the design of a parallel data-assimilation experiment is described and results from the parallel experiment are presented. Section 4 contains conclusions and describes future plans.

2. GNSS ZTD HARMONIE observation processing

a. Observations

GNSS is a satellite system that is used to pinpoint the geographic location of a user's receiver anywhere in the world. The meteorological GNSS observations are by-products of geodetic positioning with highly sophisticated estimation software packages. The microwave signals continuously broadcast by the GNSS satellites are influenced by ionospheric and neutral atmospheric effects as they travel through the atmosphere to the ground-based receivers. Using a sufficiently dense network of GNSS receivers, the impact of the neutral atmosphere in comparison with the vacuum—that is, neutral atmospheric delay—can be estimated as a by-product of the geodetic processing. These delays can be regarded as an indirect measure of the integrated water vapor along the path. The quality of the processed delay observations is insensitive to weather conditions and is very high in general, and the temporal resolution of delay observation is high as well. At the same time, the mapping of the NWP model state variables to the observed quantities might not always be so straightforward, depending on the choice of GNSS product (i.e., slant delays or ZTD). The GNSS ZTD products used in the current study were the meteorological GNSS observations that are the easiest to introduce into the variational data-assimilation scheme. They estimate the neutral atmospheric delay of a signal approaching the ground-based GNSS receiver from the local zenith direction. In reality, the GNSS ZTD observations are produced by processing a number of slant delays by utilizing satellites in the vicinity of the receiver station. Mapping functions that define the ratio between the neutral atmospheric delay at zenith and at any other elevation angle were used to produce GNSS ZTD measurements. The GNSS ZTD measurements can be translated into integrated water vapor amount in the air column just above the receiver. The disadvantage of using GNSS ZTD is a complicated observation-error structure in which both the slowly varying station-dependent observation bias and correlated observation errors are present (Kleijer 2001; Stoew 2004; Eresmaa and Järvinen 2005). Thus, as compared with assimilation of more-raw products in the form of slant delays, the assimilation of GNSS ZTD products allows for a somewhat easier mapping of NWP state variables into the observed quantities. It is therefore not necessary to take into account any slanted atmospheric ray paths and their angles, depending on atmospheric conditions. On the other hand, a more extensive handling of biases and observation errors is required. The GNSS ZTD is a measure of the integrated atmospheric refractive index n between the ground ($z = 0$) and the top of the atmosphere (TOA):

$$\int_{z=0}^{\mathrm{TOA}} [n(z) - 1]\, dz. \tag{1}$$

In a neutral atmosphere, the refractive index is dependent on pressure, temperature, and atmospheric water content. The ZTD can be decomposed into two components: the zenith hydrostatic delay (ZHD), which is proportional to the weight of a column of air per unit area (or surface pressure), and the zenith wet delay, which is related to the total precipitable water (TPW; Bevis et al. 1992, 1994). It has been demonstrated that slow (synoptic) variations reflect changes in surface pressure and TPW as air masses change when the center of low pressure passes over whereas faster variations are related to changes in TPW (Cucurull et al. 2002; Poli et al. 2007). Hence ZTD observations from the E-GVAP network of GNSS receiver stations have the potential to capture atmospheric moisture variations on short spatial and temporal scales. The GNSS ZTD observations are processed by a number of analysis centers. These centers process the data from their network of receiver stations, utilizing various software packages

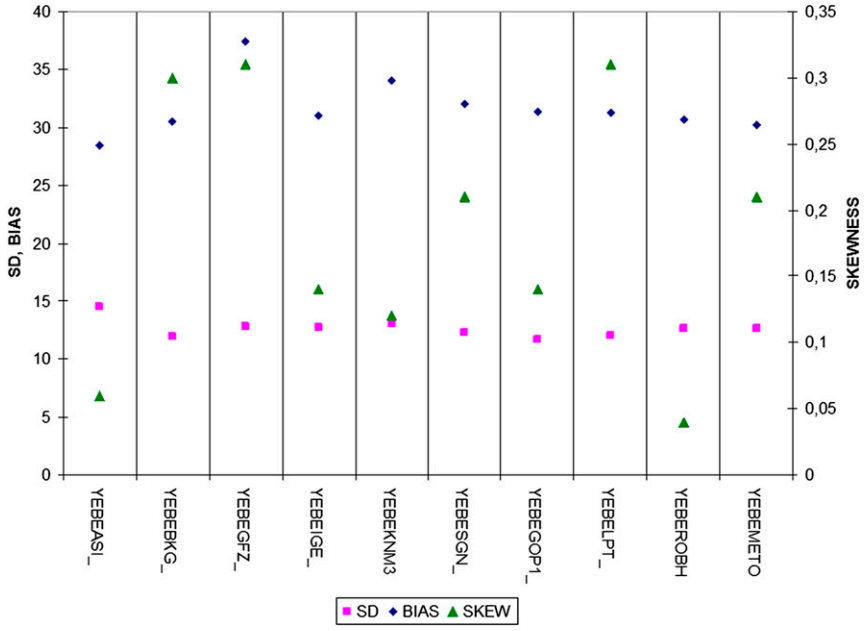

FIG. 1. Error statistics (mm) in terms of standard deviation (magenta symbols), bias (blue symbols), and skewness (green symbols) for different analysis centers that have processed the site YEBE.

such as Bernese (Dach et al. 2007) or GNSS-Inferred Positioning System and Orbit Analysis Simulation Software (GIPSY; Webb and Zumberge 1993). In addition, different processing strategies (Gendt et al. 2001; Douša 2001b,a; Douša and Bennitt 2013) that take computing resources, time constraints, and data amount into account might be applied. One individual receiver station can be processed by several different analysis centers (Bennitt and Jupp 2012; Mahfouf et al. 2015). GNSS ZTD observations from different analysis centers are collected and redistributed by E-GVAP (http://egvap.dmi.dk).

b. *Handling of redundant observations*

The HARMONIE observation-preprocessing system is designed to handle efficiently the nature of the E-GVAP network, taking into account the characteristics of individual GNSS ZTD observations. Although many GNSS analysis centers process their own national networks, there are many receiver stations that are processed by several analysis centers. On the basis of careful observation monitoring, it is possible to choose the analysis centers that provide observations of consistently suitable quality and to allow for each station only one solution for the period of study. A ''white list'' that contains the analysis center–station pairs of the best quality has been produced. The white list is based on statistics of the ZTD departures, the observation-minus-background counterpart in observation space, collected for a month previous to the period of study. The criterion for the selection of the pair into the white list was the smallest standard deviation, provided that the skewness did not exceed a predefined threshold. Departures for the white-list construction were computed from the passive run, which means that ZTD observation did enter the data-assimilation system but did not influence the analysis. The choice of the selection criterion is subjective. Note that the selection algorithm is based on statistics that reflect both observation-processing error and representativeness error. We illustrate the process of selection of the best analysis center–station pair with the example of ''YEBE'' station (Yebes, Spain), for which the ZTD observations were produced by 10 different analysis centers. Figure 1 contains ZTD departure statistics in terms of standard deviation (magenta symbols), skewness (green symbols), and bias (blue symbols) for each of the analysis centers. In this case the YEBEGOP1 pair [YEBE station produced by the ''GOP1'' analysis center (Geodetic Observatory Pecny; Czech Republic)] was chosen, being the option with the lowest standard deviation and a skewness that is less than the predefined threshold.

A second step of handling redundant information was to carry out a temporal thinning of GNSS ZTD data from the sites within the white list. Because of the high time resolution of the ZTD observations (15 min) and the relatively low assimilation frequency (3 h), we used

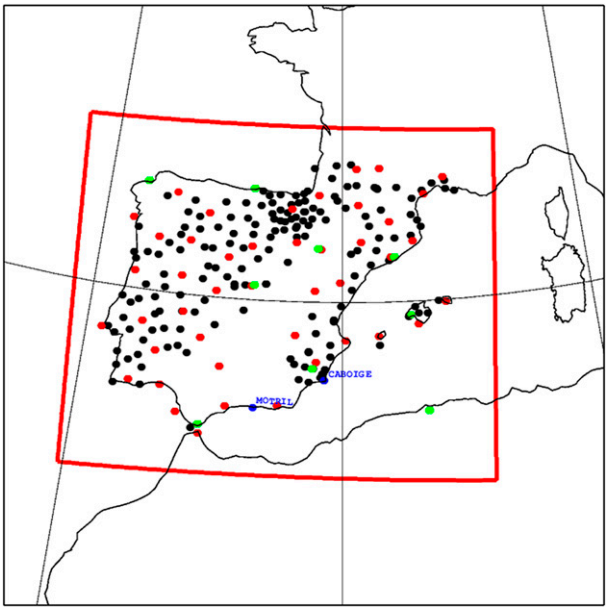

FIG. 2. Iberian Peninsula model domain (red frame) and horizontal position of GNSS ZTD observations before (black dots) and after (red dots) thinning of data. The locations of Motril and CABOIGE are marked with blue dots. In addition, the locations of the radiosonde stations that were used are marked with green dots.

only those observations from each site that were closest to the time of analysis. In this way we got rid of redundant information and concurrently minimized the persistence error that is due to the time difference between observation and analysis.

c. *Treatment of observation errors and systematic deficiencies*

In the current implementation of the HARMONIE GNSS ZTD preprocessing we employed spatial thinning to treat the correlated observation errors. We chose to apply a heavy thinning in this study: namely, an 80-km thinning distance. In this way we have mitigated the impact of correlated representativeness errors caused by, for example, orographic effects, on the initial state. Figure 2 illustrates the number of observations before and after thinning of the observations for a model domain over the Iberian Peninsula. In this way we reduced the number of observations, reduced the correlation of observation errors, and retained the most representative observations in the 3D-Var context. A more advanced preprocessing such as generation of superobservations through averaging over the time window was not tried in this study.

To treat the systematic deficiencies in assimilation of GNSS ZTD observations in the HARMONIE AROME 2.5 configuration, a bias correction was applied. The sources of bias in the ZTD observation data with respect to the ZTD model data may have been due to GNSS data-processing algorithms (use of mapping functions, formulation of hydrostatic delay, errors in the conversion of ray path to zenith delay) and systematic errors in both the model fields and the ZTD observation operator. The assimilation of observations from closely located GNSS stations can result in a model bias when no alternative unbiased sources of humidity information, such as radiosonde measurements, are available. We have noticed that the variational bias-correction coefficients described below were particularly sensitive to the bias present in closely located stations during the spinup period. This was the second reason for us to apply such severe thinning.

In particular, as described in section 2d, the relatively low model top (10 hPa) used in our HARMONIE AROME 2.5 configuration experiments will generally result in a systematically too-low model equivalent of the GNSS ZTD observations. It is obvious from Eq. (1) that the model equivalent of the integrated atmospheric refractive index computed in the HARMONIE AROME 2.5 configuration will be systematically underestimated because of the applied low model top, and the contribution to the integrated atmospheric refractive index from above the model top should be accounted for in some way. Below, we present our approach to address this problem and discuss alternative possibilities. Note that, in many of the studies cited above, global or synoptic-scale NWP models were used, usually assuming a much higher model top. For example, in Poli et al. (2007) the model top is 0.1 hPa, which approximately corresponds to an atmospheric height of 65 km. Still a systematic underestimation of the integrated refractivity index by 4–5 mm was reported, even in their study. The interpolation/extrapolation from the orography defined in the model to the real orography also contributed to systematic errors. For the HARMONIE AROME 2.5 model configuration experiments, we decided to represent the total effect of the systematic error when treating GNSS ZTD observations. One option was to carry out a static bias correction. In our study, the static bias corrections for each station in the white list were estimated from differences between the ZTD observations and the model background ZTD accumulated over a 30-day period. As an alternative to static bias correction, we also adopted and tuned an adaptive variational bias correction (VarBC) for use with GNSS ZTD observations. The VarBC coefficients are estimated within the variational data-assimilation process simultaneously with deriving the assimilation control vector and minimizing the cost function (Dee and Uppala 2009). A linear predictor model for the bias

b in the GNSS ZTD observations is applied and has the following form:

$$\mathbf{b}(\beta,\mathbf{x}) = \sum_{i=0}^{N_p} \beta_i \mathbf{p}_i(\mathbf{x}), \tag{2}$$

where $\mathbf{p}_i$ are the predictors, N_p is the number of predictors, and β_i are the unknown bias parameters. Estimating the bias parameters is achieved by including them in the control vector for the variational data assimilation, which results in a cost function of the following form:

$$J(\mathbf{x},\beta) = 0.5(\mathbf{x}-\mathbf{x}^b)^{\mathrm{T}}\mathbf{B}^{-1}(\mathbf{x}-\mathbf{x}^b) + 0.5(\beta-\beta^b)^{\mathrm{T}}\mathbf{B}_\beta^{-1}(\beta^b) + 0.5[H\mathbf{x}+b(\mathbf{x},\beta)-\mathbf{y}]^{\mathrm{T}}\mathbf{R}^{-1}[H\mathbf{x}+b(\mathbf{x},\beta)-\mathbf{y}]. \tag{3}$$

Here $\mathbf{x}$ is the initial model state, to be estimated simultaneously with the bias parameters β. Furthermore, $\mathbf{x}^b$ and β^b are the background model state and the background bias parameters, respectively. The observations are denoted by $\mathbf{y}$, and H is the observation operator that transforms the model state into the observed quantities. Also, $\mathbf{B}$, $\mathbf{B}_\beta$, and $\mathbf{R}$ are the error covariance matrices for the model background state, the background bias parameters for the predictors, and the observation-error covariances, respectively. In our current implementation we update the VarBC coefficients every 3 h. We parameterize the total value of systematic differences between GNSS ZTD observations and their model equivalent as a station-dependent offset parameter, that is, one single constant value per station. The stiffness, or adaptivity of the GNSS ZTD VarBC, has been tuned by sensitivity studies. The functionality of the variational bias correction is illustrated by the time evolution of bias-correction coefficient and observation-minus-background counterpart departures, as well as observation and model equivalents for one particular station ("CABOIGE"; 37.6°N, 0.7°W) during a preparatory period during which the GNSS ZTD observations entered the system in passive mode only and did not influence the model's initial state (Fig. 3). It can be seen that the variational data-assimilation scheme is able to correct the observations for the systematic differences at this particular site with an adaptivity time of 7–10 days. This implies that the bias was removed after roughly 70 updates of the bias-correction coefficients, taking into consideration that there were eight data-assimilation cycles each day. The illustrated adaptivity corresponds to a stiffness coefficient in the variational bias-correction scheme equal to 25, which was used in our study. The design of an enhanced variational bias-correction scheme for assimilation of GNSS ZTD is ongoing; we aim to introduce additional predictors.

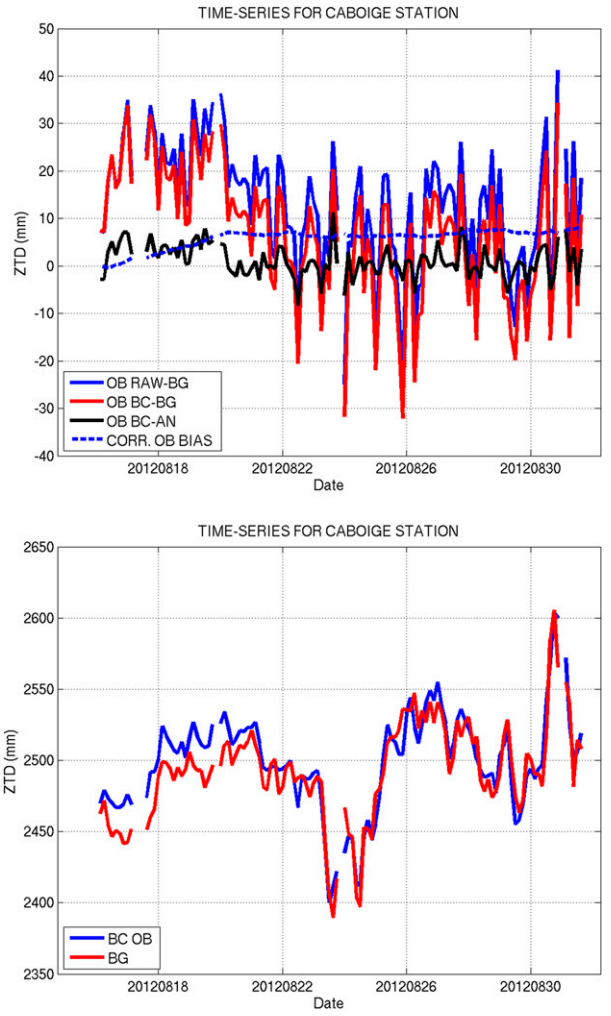

FIG. 3. Time series (mm) from GNSS ZTD site at CABOIGE: (top) departure (observation minus background) before (blue solid line) and after (red solid line) VarBC, estimated observation bias to be corrected (blue dashed line), and bias-corrected departure (observation minus analysis; black solid line) and (bottom) the bias-corrected observation (blue solid line) and model state background equivalent (red solid line).

The GNSS ZTD observation errors of the observations accepted for the data assimilation were assumed to have a Gaussian error distribution with an observation-error standard deviation of 20 mm. This observation-error standard deviation was derived from observation-minus-background and observation-minus-analysis departures, and it was empirically adjusted so that less weight was given to the observation than to the background. Objective methods such as the one proposed by Desroziers et al. (2005) could be tried instead to tune the observation-error variance.

Observations affected by gross errors may significantly degrade the initial state and the resulting forecast if not taken into account. In our system, gross errors were identified and removed by a first-guess check. In this check, the background model state $\mathbf{x}^b$ was projected on the observed quantity y_i with the observation operator H (see section 2d below). The squared background departure from the observation i was calculated and the observation y_i was rejected if it did not satisfy the following inequality:

$$\{[H(\mathbf{x}^b)]_i - y_i\}^2/\sigma^2_{b,i} > L\lambda, \tag{4}$$

where $\lambda = 1 + \sigma^2_{o,i}/\sigma^2_{b,i}$, L is the rejection limit, $\sigma^2_{o,i}$ is the observation-error variance, $\sigma^2_{b,i}$ is the background-error variance, and $[H(\mathbf{x}^b)]_i$ denotes the projection of the model state on observation i. In the first-guess check, a background-error standard deviation of roughly 10 mm was used. The rejection limit for GNSS ZTD observations in the HARMONIE AROME 2.5 model configuration was empirically set to 4. This value resulted in a relatively strict background quality control of GNSS ZTD observations.

In the minimization of the cost function within the variational data assimilation, the background-error variance is dependent on the background-error statistics of the data-assimilation control variable, which is specified in terms of vorticity, unbalanced divergence, unbalanced temperature, unbalanced specific humidity, and unbalanced surface pressure (Derber and Bouttier 1999; Berre 2000). The climatological background-error statistics used in the current study were derived from an ensemble of HARMONIE forecast differences obtained through downscaling of ECMWF Ensemble Data Assimilation (EDA)-based forecast fields. To be specific, the ECMWF EDA–based forecast fields were horizontally and vertically interpolated to the HARMONIE AROME 2.5 configuration geometry and used as initial conditions for high-resolution nonhydrostatic model runs. The ECMWF EDA uses a T399 horizontal resolution and 91 vertical levels. Then the evolved high-resolution ensemble was scaled to be consistent with the amplitude of the 3-h forecast error for HARMONIE AROME 2.5. The values applied correspond roughly to a GNSS ZTD background-error standard deviation of 10 mm and are thus consistent with the one applied in the first-guess check.

d. Observation operator

The observation operator projects the model state on the GNSS ZTD observation. Because a variational framework was used, nonlinear as well as corresponding tangent linear and adjoint versions of the observation operator were needed. The ZTD observation operator H, given a station location (including altitude), calculated the model equivalent of the GNSS ZTD by vertically integrating the modeled refractivity from the station height to the model top. The GNSS ZTD observation operator used in our study was to a large extent based on that described in Poli et al. (2007). An alternative formulation is possible, however, as, for example, in Vedel and Huang (2004). As we have already mentioned above, the low model top will result in systematic underestimation of the model equivalent of the GNSS ZTD. The contribution from above the model top should be accounted for in some way. We have followed the ideas suggested by Poli et al. (2007) and have included the contribution from above the model top as part of the systematic deficiencies. Poli et al. (2007) used a static approach for bias estimation, computing the bias offline through a moving window, one offset parameter per station. The novelty of our approach is that a variational bias correction is used for these purposes, when the offset parameters are estimated online through variational techniques. An alternative approach is to estimate the contribution to the delay above the model top analytically (see, e.g., Bennitt and Jupp 2012; Yan et al. 2009a). We have extended the capability of the GNSS ZTD observation operator, introducing an analytical approach to account for the delay above the model top, following the approach described in Vedel et al. (2001). The estimated contribution to the delay from above the model top in the HARMONIE AROME 2.5 configuration is on the order of 20 mm, which is consistent with the results reported in other studies, taking into account the low model top that is assumed in the HARMONIE AROME 2.5 configuration.

3. Design of parallel experiment

a. Model setup

Three extended parallel data-assimilation-and-forecast experiments were performed with the HARMONIE AROME 2.5 model configuration on a domain that is centered on the Iberian Peninsula, shown as the red outline in Fig. 2. The horizontal grid resolution was 2.5 km, and there were 65 vertical model levels extending up to 10 hPa. Both upper-air (Seity et al. 2011) and surface data assimilations (Giard and Bazile 2000; Mahfouf et al. 2009) were applied to obtain the best possible initial model state. The climatological background-error statistics for the upper-air data assimilation were derived from an ensemble of HARMONIE forecast differences, obtained through downscaling of the ECMWF EDA analyses and forecast fields. This approach is in fact suboptimal because it might require more than 12 h of model

integration to establish realistic convective-scale spectra when the high-resolution model is initialized from the ECMWF coarse-resolution fields (N. Gustafsson 2015, personal communication). We have decided to use this approach for generation of the structure functions, despite its suboptimality, because the main aim of our study was to investigate the potential of assimilating the GNSS ZTD observations into the configuration as closely as possible to the approach used for operations by the HIRLAM consortia. It should also be taken into account that 3D-variational data assimilation is performed in spectral space and assumes homogeneous and isotropic forecast-error structures. Such an assumption is far from reality when describing convective-scale phenomena and moist processes in particular. The assimilation of GNSS ZTD observations using flow-dependent forecast-error covariances, employing a 4D-variational data assimilation or hybrid ensemble variational techniques, is a subject for future study.

The forecast model is described in detail in Seity et al. (2011). It has a spectral representation and a nonhydrostatic formulation. Stratiform and deep convective clouds are explicitly represented, and for shallow convection a subgrid parameterization is applied using an eddy-diffusivity mass flux scheme (Rooy and Siebesma 2010). The representation of the turbulence in the planetary boundary layer is based on a prognostic turbulent kinetic energy equation combined with a diagnostic mixing length (Cuxart et al. 2000). For radiative transfer, the shortwave spectrum is described with six spectral bands (Fouquart and Bonnel 1980) and the longwave radiation is modeled in accordance with Mlawer et al. (1997). Surface processes are modeled using the SURFEX (Masson et al. 2013). Lateral boundary conditions were provided by 3-hourly ECMWF operational forecasts. In addition, a spectral large-scale mixing of the background state, the 3-h HARMONIE forecast fields, with the lateral boundary ECMWF fields was applied. In this way we hoped to benefit from the high-quality large-scale information from the ECMWF global forecasts in the regional HARMONIE data assimilation. The main characteristics of the model setup are summarized in Table 1.

TABLE 1. Setup of modeling system.

Component	Option applied
Surface data assimilation	Optimal interpolation
Observation usage, surface	SYNOP
Upper-air data assimilation	3D-Var
Observation usage, upper air	Conventional and GNSS
Forecast model	AROME
Lateral boundary conditions	3-hourly ECMWF forecasts

b. *Experimental design*

The HARMONIE AROME 2.5 configuration of the forecasting system was run with a 3-h data-assimilation cycle for the period 1–30 September 2012 and with a 2-week spinup period before that. This particular month was chosen because it was characterized by several heavy-precipitation events associated with moist and warm weather conditions. We expect that additional moisture-related observations should be particularly beneficial for prediction of such weather situations. We ran short-range forecasts every 3 h to provide the background of the next analysis, and we launched forecasts up to 36 h 4 times per day. We have conducted three parallel experiments that differed in whether GNSS ZTD observations were used and in the bias-correction method that was applied for ZTD GNSS data. These three parallel experiments are abbreviated as follows:

1) CRL (the control run) indicates assimilation of only conventional in situ observations in the upper-air data assimilation.
2) STA indicates assimilation of conventional in situ observations and GNSS ZTD observations in the upper-air data assimilation, with a static bias correction applied to the GNSS ZTD observations.
3) VBC indicates assimilation of conventional in situ observations and GNSS ZTD observations in the upper-air data assimilation, with VarBC applied to the GNSS ZTD observations.

Note that CRL differed from STA and VBC in data usage only. On the other hand, STA differed from VBC in the method applied for bias correction for GNSS ZTD observations. Thus we could investigate both the impact of using GNSS ZTD observations and the sensitivity to the choice of method for bias correction of GNSS ZTD observations. The GNSS ZTD observations were taken from the E-GVAP data archive. The bias-correction coefficients for five selected stations from different parts of Spain are presented in Table 2 for the spinup and assimilation period. For all stations, the variational bias-correction coefficients did have a significant variation within the period. The static bias-correction values can be seen to fall within the range of values obtained with variational bias correction, however. The conventional in situ observations used in the upper-air data-assimilation include radiosonde, pilot-balloon wind, SYNOP, ship, and aircraft measurements, and these were obtained from the ECMWF Meteorological Archival and Retrieval System (MARS).

To evaluate the relative quality of the analyses and subsequent forecasts from the different parallel experiments, we verified them against radiosonde and SYNOP

TABLE 2. GNSS ZTD bias-correction coefficients (m) for a selection of stations.

Station identifer	Lat (°N)	Lon (°E)	Alt (m)	STA	VBC (14 Aug)	VBC (28 Aug)	VBC (14 Sep)	VBC (28 Sep)
BCLNIGE	41.40	2.00	35.0	0.034 72	0.0301	0.0289	0.0355	0.0374
BERGIGE	40.61	−0.10	841.0	0.030 50	0.0253	0.0308	0.0354	0.0333
CDRDIGE	40.59	−6.54	623.0	0.031 76	0.0315	0.0297	0.0320	0.0319
JORDIGE	39.31	3.00	9.0	0.028 54	0.0206	0.0289	0.0342	0.0359
OLMEIGE	41.28	−4.68	775.0	0.028 07	0.0266	0.0259	0.0311	0.0328

observations within the model domain. The verification was carried out for weather parameters at the surface level and for the upper-air parameters, wind, temperature, and humidity. The model data used in the statistics were the analyses and forecasts of up to 24 h. Special emphasis was put on verification of humidity and precipitation. The objective statistical verification was also complemented with a more subjective verification for individual cases.

c. *Verification scores of parallel experiments*

In Fig. 4 bias and root-mean-square error (RMSE) verification scores averaged over the whole period are shown for the three parallel experiments CRL, STA, and VBC. For temperatures the scores were similar for the three experiments. On the other hand, the RMSE scores for wind differed among the three runs. There was a neutral to slightly positive impact from utilizing GNSS ZTD observations if VarBC was applied. If a static bias correction was applied, the RMSE scores became larger than for the CRL experiment. The assimilation of the GNSS ZTD observations while applying the static bias-correction scheme (STA experiment; blue curves) increased both the bias and the RMSE of the relative humidity forecasts measured against radiosonde data in comparison with the control run (CRL experiment; red curves). At the same time the assimilation of the GNSS ZTD observations while applying the variational bias-correction scheme (VBC experiment; green curves) reduced RMSE of the relative humidity while keeping the bias almost unchanged when compared with CRL. Note that the bias verification scores indicate that the low-tropospheric humidity forecasts were associated with a wet bias and that the low-tropospheric temperature forecasts were associated with a cold bias.

We have investigated further the reason for degradation of the relative humidity scores when assimilating the GNSS ZTD observations while applying the static bias correction. In Fig. 5 we show observations-minus-background statistics of radiosonde tropospheric humidity observations assimilated in the study for these three experiments. Although the observations were the same, the background fields were different for the three experiments. They were the 3-h forecasts of specific humidity assimilating conventional observations only (CRL; blue curves) and assimilating the GNSS ZTD while in addition applying the static bias-correction scheme (STA; red curves) or the variational bias-correction scheme (VBC; green curves). The STA experiment produced a too-wet specific humidity background field in comparison with the radiosonde data (Fig. 5, top panel) and slightly increased the RMSE (Fig. 5, bottom panel) relative to the CRL experiment; the VBC experiment produced a slightly smaller RMSE of specific humidity, in particular at levels around 700 hPa, while keeping the bias unchanged.

Verification figures for the 12-h accumulated precipitation forecasts by the Kuiper skill score (KSS) are shown in Fig. 6 for September of 2012. The KSS is a combination of the hit-rate and the false-alarm skill scores and is shown here for the classes of 0.01, 0.3, 1.0, 3.0, 10.0, and 100.0 mm $(12\,\text{h})^{-1}$. KSS values of 1.0 indicate a perfect forecast, and values of 0.0 indicate no skill. Figure 6 shows that a neutral to positive impact of assimilating GNSS ZTD observations can be found. This positive impact was mainly associated with improved prediction of higher precipitation rates when utilizing GNSS ZTD observations and was most pronounced when applying a variational bias correction to GNSS ZTD observations.

d. *Case studies*

The three different precipitation forecasts were verified against SYNOP observations in a list made for Spain–Portugal using 115 stations. This analysis can be considered to be a close representation of the actual conditions over Iberia. Figure 7 shows the time series of the forecast verification scores for 12-h accumulated precipitation (24 h − 12 h) from HARMONIE over the Iberian domain. For the majority of the cases over the study period, the scores of the 12-h accumulated precipitation forecasts were very similar for the CRL, STA, and VBC experiments, but there were a few exceptional cases with larger differences. For example, for the forecasts valid at 1200 UTC 8 September 2012 VBC was clearly better than CRL and STA in terms of the verification scores.

At this time a rainy band was present just north of Lisbon, Portugal (38.5°N, 9.1°W) (Fig. 8). In the CRL

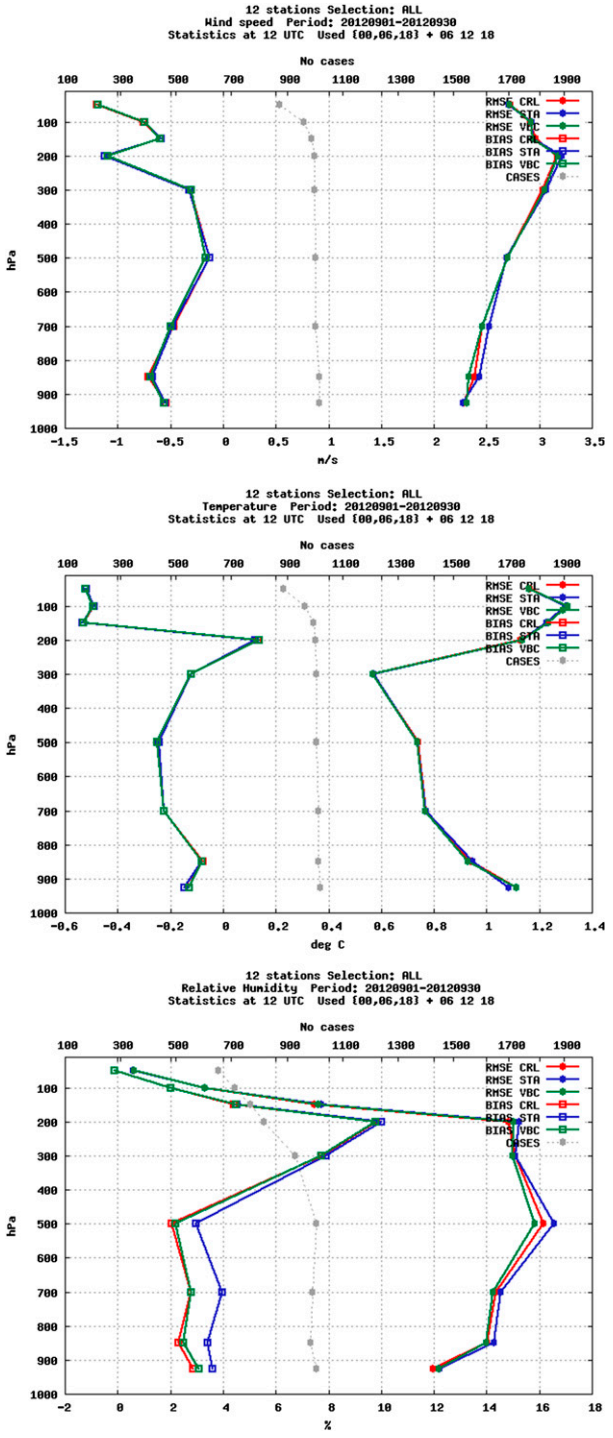

FIG. 4. Verification of forecasts of (top) wind speed ($m\,s^{-1}$), (middle) temperature (K), and (bottom) relative humidity (%) against 12 radiosonde stations over a Spain–Portugal area for September 2012. The red curves are for CRL, blue curves are for STA, and green curves are for VBC. The scores include 6-, 12-, and 18-h forecast ranges.

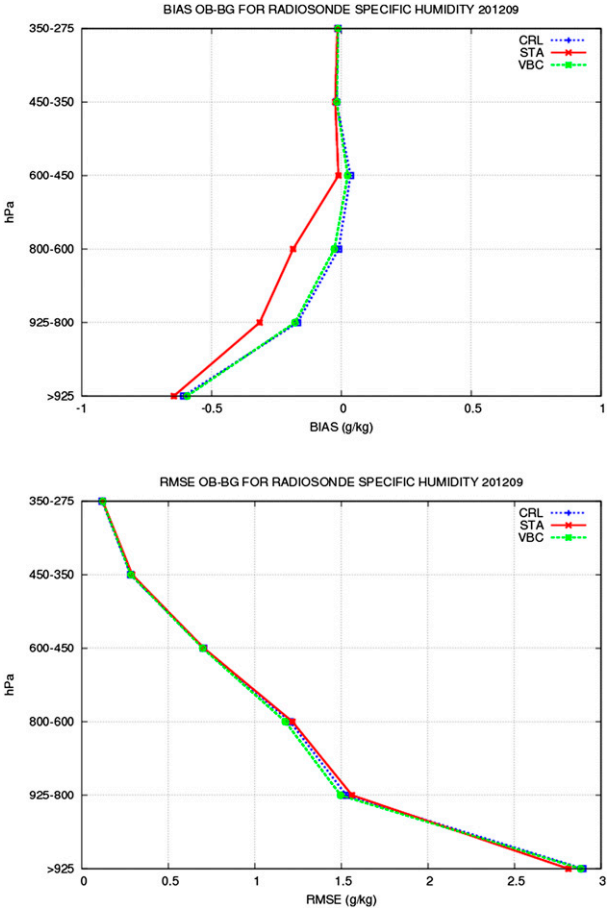

FIG. 5. (top) Bias and (bottom) RMSE of observation-minus-background specific humidity departures from tropospheric radiosonde humidity observations ($g\,kg^{-1}$) assimilated during the experiment for September 2012. The blue curves are for CRL, red curves are for STA, and green curves are for VBC.

experiment (Fig. 8a), HARMONIE has the capacity to simulate the rainy system. The rainy band in the VBC experiment (Fig. 8b) had a similar orientation and intensity but was narrower, and the overall precipitation was reduced in accordance with the observed 12-h precipitation. The STA experiment had a verification score that was similar to that of CRL and is therefore not shown here.

The impacts on wind and specific humidity differences (q24d; Figs. 9a,c) and on temperature differences (T24d; Figs. 9b,d) between the CRL (no ZTD) and the VBC (ZTD VarBC) at model levels 33 (located approximately at 700 hPa; Figs. 9a,b) and 45 (located approximately at 900 hPa; Figs. 9c,d) for the 24-h forecast from 1200 UTC 7 September 2012 are shown in Fig. 9. Notice here in the CRL experiment, relative to both the VBC experiment and the precipitation scores (Fig. 7), the overprediction of the specific humidity (q; difference of

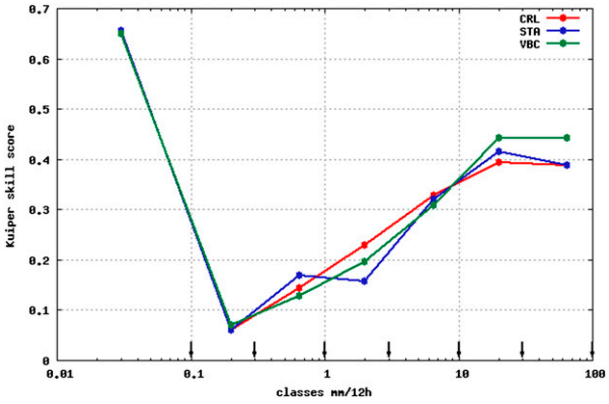

FIG. 6. Verification of 12-h accumulated precipitation forecasts with the KSS against SYNOP stations using 115 stations for September 2012. The red, blue, and green curves are for CRL, STA, and VBC, respectively.

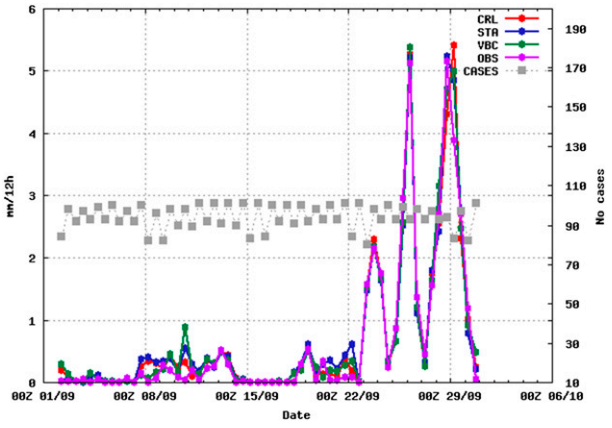

FIG. 7. Time series of verification scores for the 12-h accumulated precipitation forecasts and SYNOP observations using the Spain–Portugal list of 115 stations for the CRL (red curve), STA (blue curve), and VBC (green curve) experiments over an Iberian area for September 2012. The numbers of cases are shown by gray squares.

over 1 g kg^{-1}) and also how low the temperature was on an east–west rainband just north of Lisbon at model level 45 and in the large-scale flow over western Iberia at model level 33. Thus in this large-scale flow the VarBC ZTD experiment revealed the impact seen in the precipitation score. We note also that the humidity variations partly took place on small scales as compared with the GNSS ZTD data used after thinning and the length scales of our applied background-error statistics.

We tracked these forecast differences back to the analysis differences. The specific humidity analysis increment (qincr) patterns at 1200 UTC 7 September are presented in Fig. 10 for CRL (Figs. 10a,c) and VBC (Figs. 10b,d) at model levels 33 (Figs. 10a,b) and 45 (Figs. 10c,d). Notice that the variational bias correction dried the model more than did CRL, such that the impact of assimilating GNSS ZTD observations together with VarBC managed, in this case, to dry out a too-wet model near the rainband. Although different background states were used in the two different experiments, these differences were evident also when comparing the analysis fields of the two runs (not shown). We conclude that these large differences in the analysis of humidity between the CRL and the VBC over western Iberia were due to the assimilation of GNSS ZTD in VBC. Furthermore, these differences in the humidity analysis were mainly responsible for the differences in the forecasts between CRL and VBC over western Iberia 1 day later. Note also the substantially larger spatial scales in the increments of the humidity analysis (Fig. 10) as compared with the spatial scales in the rainband (Fig. 8). This was due to simplifying assumptions (such as isotropy and homogeneity) in the currently applied background-error statistics. Our plans include alleviating these limiting assumptions.

Another interesting event took place at 0600 UTC 28 September 2012. Around this time there was a developing weather system with associated precipitation in the middle and southern part of Spain, as revealed in the radar reflectivity (dBZ) PPI image shown in Fig. 11. The precipitation system was moving from the western part toward the eastern part of Spain. Also shown in Fig. 11 are the model-simulated reflectivity maps (at 300-m height) for the 6-h forecasts valid at the same time as the radar image for the three parallel experiments. By comparing the CRL model-simulated reflectivity map with the radar image, one can see that it severely overpredicted the precipitation event just offshore of the town of Motril (36.75°N, 3.35°W) on the Mediterranean coast of Spain. The precipitation event offshore of Motril was significantly better captured by VBC and, in particular, STA. Furthermore, the precipitation amounts in the northern part of Spain were heavily overpredicted by CRL. The VBC and STA precipitation amounts in northern Spain were also too high but were substantially lower than in CRL, as illustrated in Fig. 12. There also was a large precipitation system over Morocco and the southwestern part of Spain (Fig. 11). This latter system was missed by all of the parallel runs.

We may speculate that the reason why the data assimilation failed to capture this rapidly developing event was the very close southerly model lateral boundary in combination with the northeasterly flow and the lack of assimilation of humidity data over the sea, such as AMSU-A Microwave Humidity Sounder (MHS) satellite data. At the same time, the reason for the improved

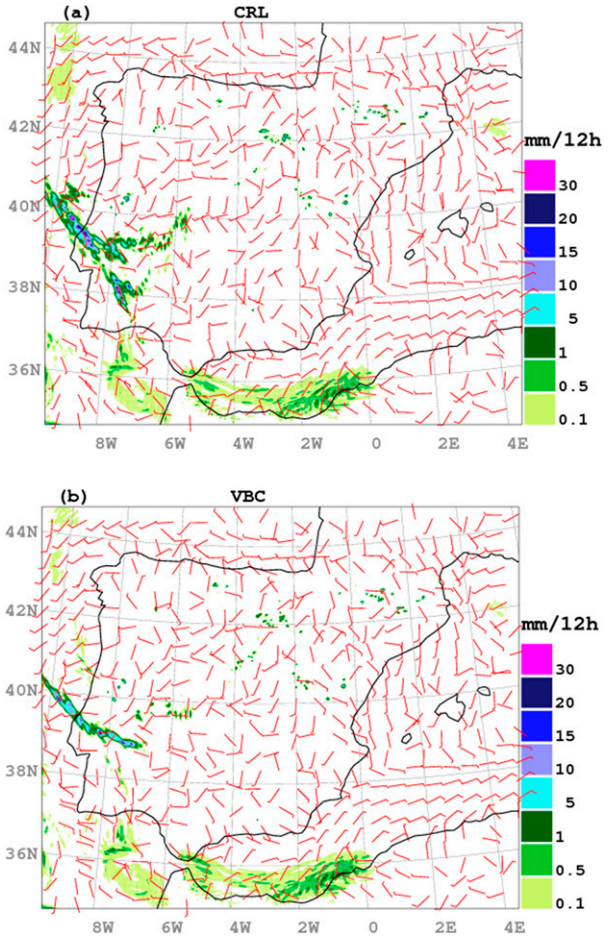

FIG. 8. Simulations of 12-h accumulated precipitation forecasts [24 h − 12 h; mm (12 h)$^{-1}$; color shades] and wind barbs representing 10-m wind forecasts starting at 1200 UTC 7 Sep 2012: (a) at +24 h from the CRL run and (b) at +24 h from the VBC run.

precipitation forecast offshore of Motril and in northern Spain can be attributed to the assimilation of GNSS ZTD observations. To illustrate this, the model level-33 specific humidity analysis and analysis increments for CRL and VBC at 0000 UTC 28 September 2012 are shown in Fig. 13. Also shown is the analysis difference of specific humidity at model level 33, together with the analyzed wind field at the same vertical level. The CRL analysis increments resulted mainly from radiosonde humidity observations, and the increments were positive along the Mediterranean coast of Spain. The analysis moistened the model background state in the lower troposphere along the Mediterranean coast of Spain. In northern Spain, the increments were neutral to negative and the analysis acted to slightly dry the model background state in the lower troposphere. The VBC analysis increments, on the other hand, resulted from both radiosonde humidity observations and GNSS ZTD observations from the network of GNSS sites used (Fig. 2). From Fig. 13 it can be seen that the VBC analysis increments were in fact negative along the entire southwestern part of Spain, extending all the way to the western part of the Mediterranean coast. These drying effects of the lower-tropospheric part of the background field in the southwestern part of Spain, due to the GNSS ZTD observations, together with the southwesterly flow, resulted in a better-forecast precipitation event 6 h later offshore of Motril. In addition it is evident that the analysis increments in the northern part of Spain had more negative values for VBC than for CRL. The GNSS ZTD observations enforced the drying effect of the analysis in the northern part of Spain. This was the reason for the improved precipitation amounts in the 6-h forecast of VBC, as compared with CRL, in the northern part of Spain. We also stress that the HARMONIE forecasts over the Iberian Peninsula for the period of our study apparently suffer from a persistent negative surface pressure bias associated with a systematically too-cold or too-wet air mass. The reason for this biased HARMONIE AROME 2.5 behavior is under investigation. It is very difficult to assimilate the observations into the model with the wrong climate. In this view, the ability of the GNSS ZTD observations to reduce the model bias and to improve the quality of the HARMONIE forecast looks even more encouraging. This gives us hope that assimilating more observations will help to constrain the HARMONIE AROME 2.5 model configuration and construct the initial state, which will then result in a more realistic forecast, even if the model climate is not perfect.

4. Conclusions and future plans

The HARMONIE kilometer-scale short-range numerical weather forecasting system has been prepared for assimilation of GNSS ZTD observations. The observation-handling system includes data selection, bias correction, quality control, and a GNSS ZTD observation operator for data assimilation. The functionality of the different components was investigated in detail along with the overall performance of the GNSS ZTD data assimilation. It has been proven successful in assimilating GNSS ZTD in our HARMONIE AROME 2.5 experiments, despite the relatively low model top used in our model configuration. An extensive observation preprocessing and treatment of systematic differences between observed values and their model equivalents were required, however. In this paper, we have chosen to treat the contribution to the integrated simulated refractivity index from above the model top as one component contributing to the systematic differences

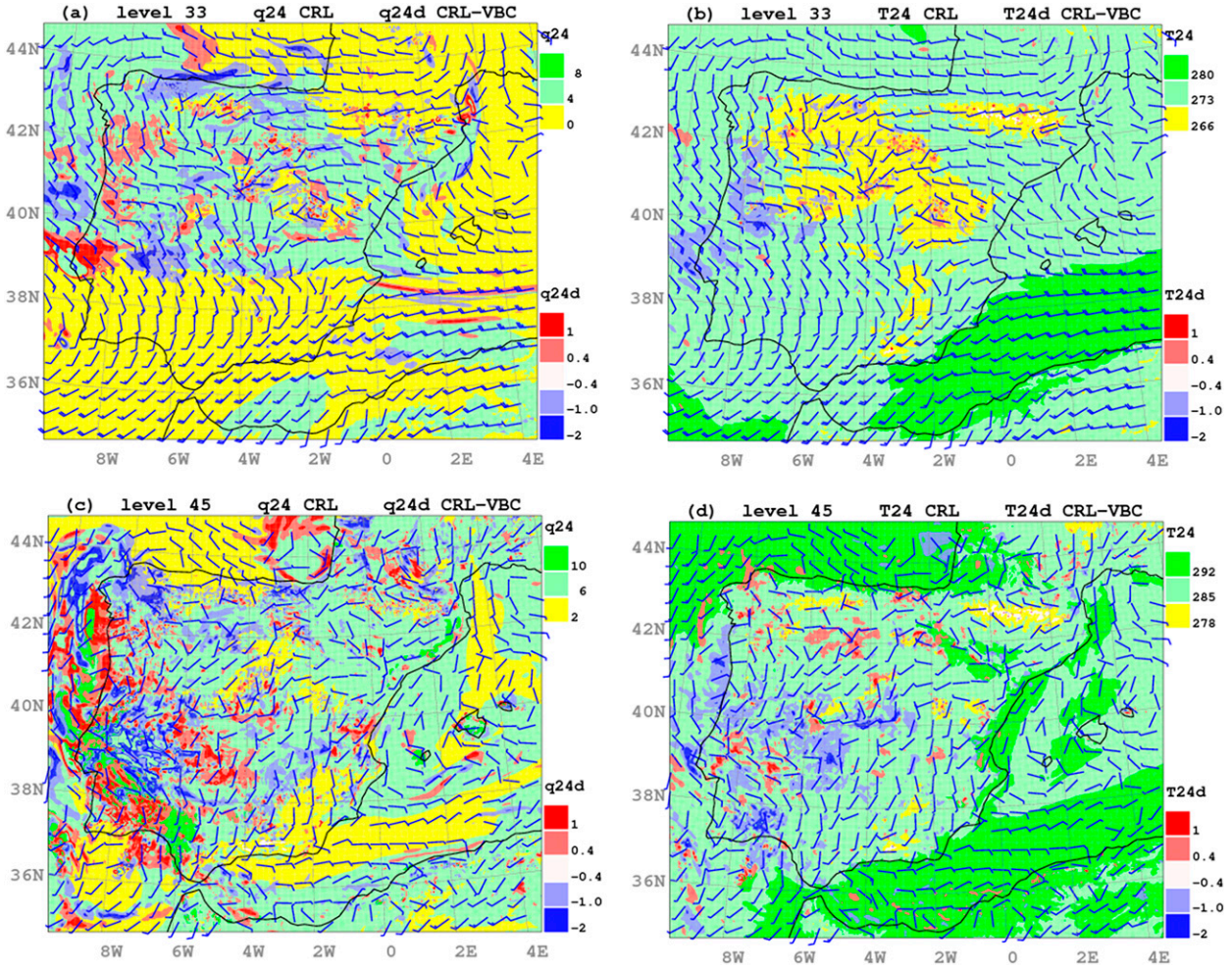

FIG. 9. Simulations starting at 1200 UTC 7 Sep 2012, with all panels showing results for +24 h, at model levels (top) 33 and (bottom) 45 for (a),(c) simulated specific humidity (q24) forecasts (g kg^{-1}) for CRL, specific humidity forecast differences (q24d; g kg^{-1}) between CRL and VBC, and wind barbs representing wind forecasts for CRL and for (b),(d) temperature (T24) forecasts (K) for CRL, temperature forecast differences (T24d; K) between CRL and VBC, and wind barbs representing wind forecasts for CRL. Note that the wind barb fields in the humidity and temperature panels are identical at each model level.

between the modeled and observed GNSS ZTD values. We have decided to parameterize these systematic differences as a station-dependent offset parameter, and we used the variational bias-correction device to estimate these parameters online. Our experiences are of relevance for other model setups focusing on the lower part of the atmosphere and having a relatively low model top. An alternative would be to explicitly account for the part of the GNSS ZTD above the model top within the observation operator. The contributions of this paper concern a comprehensive GNSS ZTD observation-handling system, including VarBC, as well as detailed analyses of the impact of GNSS ZTD data, both in terms of statistical evaluations over a longer period and in terms of individual case studies.

The benefits of a variational bias correction as compared with a static bias correction have been demonstrated. Use of GNSS ZTD observations together with a variational bias correction has been shown to improve short-range weather forecasts, both statistically and in individual case studies. The improvements are mostly due to the ability of the GNSS ZTD observations to dry a too-wet model state and therefore to improve precipitation scores. Our work on assimilation of GNSS ZTD observations into a kilometer-scale forecasting system has helped us to outline several important aspects of kilometer-scale data assimilation. First of all, a systematic tuning of the data-assimilation system on the basis of objective validation methods has been shown to be required so as to obtain a positive impact from newly introduced observations. We have also seen that even in

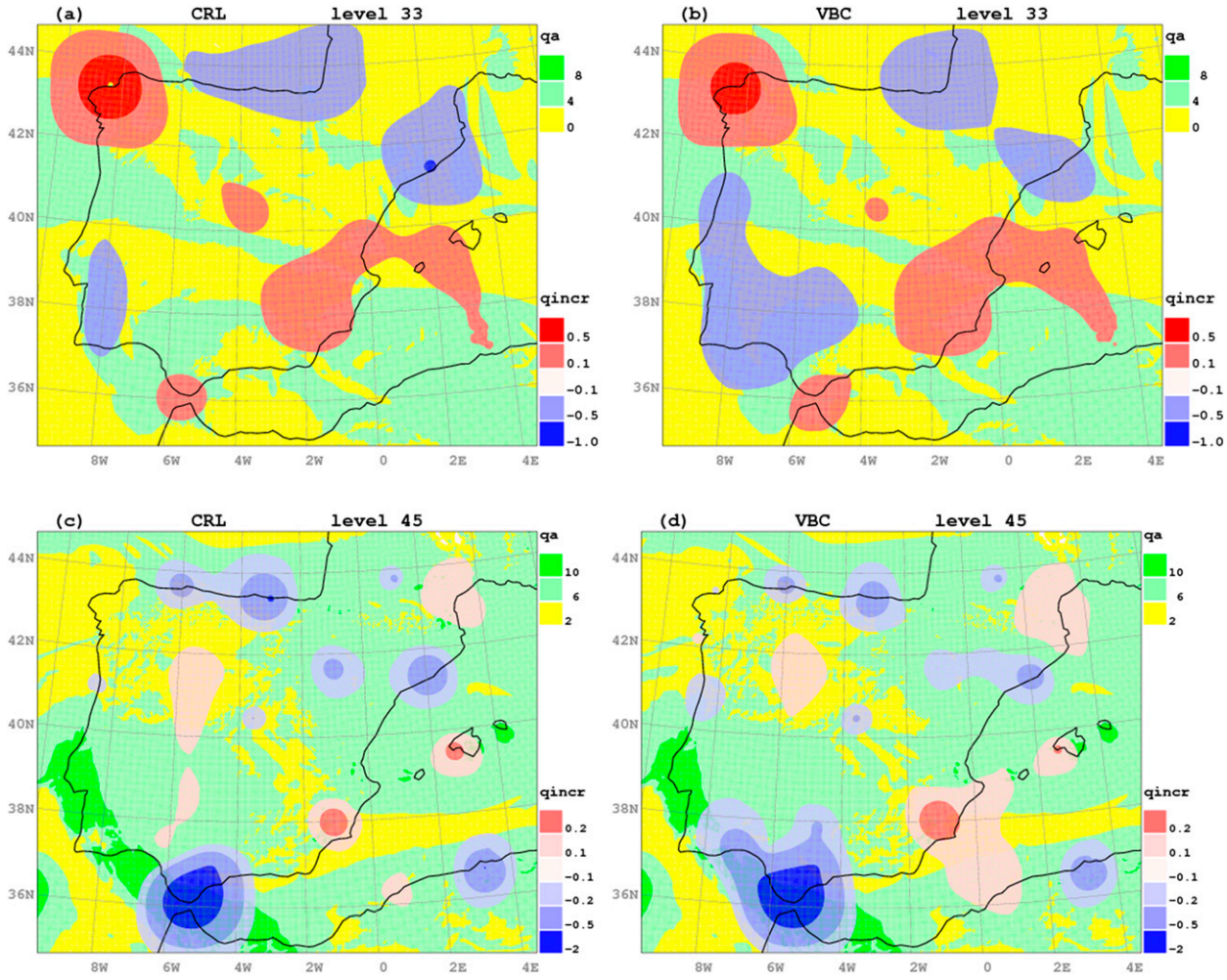

FIG. 10. Analysis increments (qincr) and analysis (qa) of specific humidity (g kg^{-1}) for the (a),(c) CRL and (b),(d) VBC experiments at model levels (top) 33 and (bottom) 45 for 1200 UTC 7 Sep 2012.

the case of biased model behavior it is possible to improve the forecast quality by assimilating observations when the model is fed these observations with care. In this case the improved forecast scores do not necessarily mean improved analysis scores. Second, our work on the assimilation of high-resolution GNSS ZTD observations has revealed that the HARMONIE AROME 2.5 data-assimilation system is still far from being optimal for kilometer-scale data assimilation. The HARMONIE 3D-Var system was to a large extent built on the one developed for synoptic scales. The HARMONIE 3D-Var uses climatological background-error statistics that are derived from the ensemble of host model perturbations, downscaled through a 6-h HARMONIE forecast model integration. It is assumed that the background-error statistics are homogeneous and isotropic and that the linear balance assumption holds. These assumptions do have weaknesses. Our investigations have shown that the background-error statistics used in our study contained very little energy on small scales. An alternative technique for generation of climatological background-error statistics with more energy at scales below 100 km is under development. This will allow better utilization of the potential of high-resolution observations.

Our work has revealed several ideas for further work and enhancements regarding assimilation of GNSS ZTD observations. Emphasis will be on further investigation and possible modeling of GNSS ZTD spatial and temporal observation-error correlations. This would enable us to reduce the large thinning distance of 80 km. Introduction of more predictors, such as layer thickness, into the VarBC should further enhance the GNSS ZTD VarBC. Because moisture variations in a kilometer-scale model are relatively small scale and vary significantly from day to day it is most likely that humidity data assimilation would

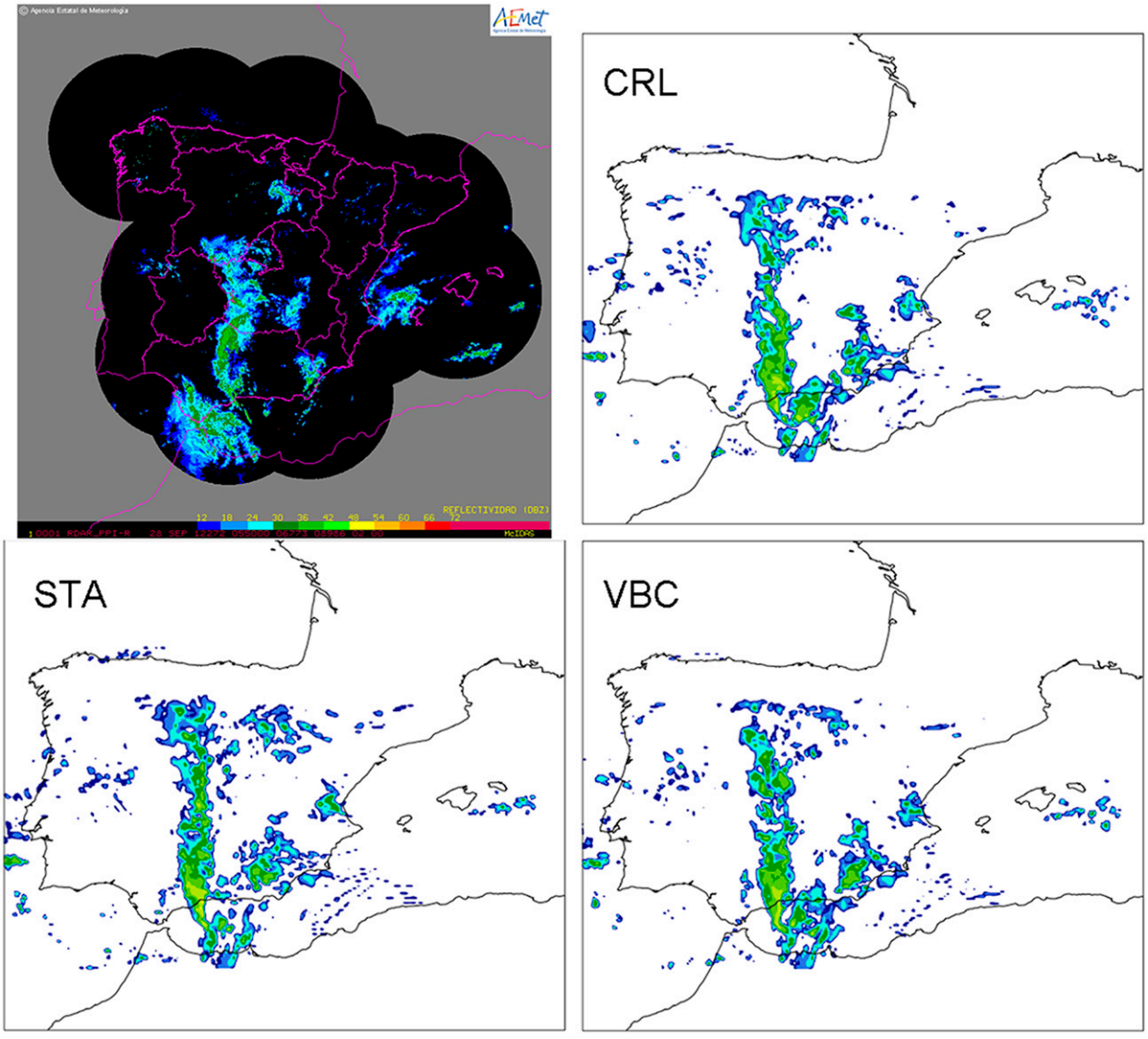

FIG. 11. (top left) PPI radar reflectivity image (dB*Z*) at 0550 UTC 28 Sep 2012, along with maps of simulated reflectivity at 300 m (dB*Z*) for the 6-h forecast from 0000 UTC 28 Sep 2012, valid at 0600 UTC 28 Sep 2012, for (top right) CRL, (bottom left) STA, and (bottom right) VBC.

benefit significantly from flow-dependent background-error statistics. It is among our future plans to refine the forward observation operator for GNSS ZTD observations that was used in our study, in particular the interpolation/extrapolation from the model orography to the station orography, and to combine assimilation of GNSS ZTD observations together with other sources of humidity observations, such as the AMSU-A MHS instrument, to investigate the combined impact and interactions.

Acknowledgments. This research study has been done as part of the COST Action ES1206. We are grateful to the E-GVAP Program for providing GNSS ZTD observations and to Henrik Vedel for sharing his experiences about the nature of these observations. The support from Roger Randriamampianina and Paul Poli for the adoption of variational bias correction to GNSS ZTD observations is greatly appreciated. The HARMONIE AROME 2.5 model configuration is being jointly developed by the ALADIN and the HIRLAM consortia and is specifically targeted for convection-permitting scales. The ALADIN and HIRLAM consortia join 26 National Weather Services in Europe and North Africa: Algeria, Austria, Belgium, Bulgaria, Croatia, Czech Republic, Denmark, Estonia, Finland, France,

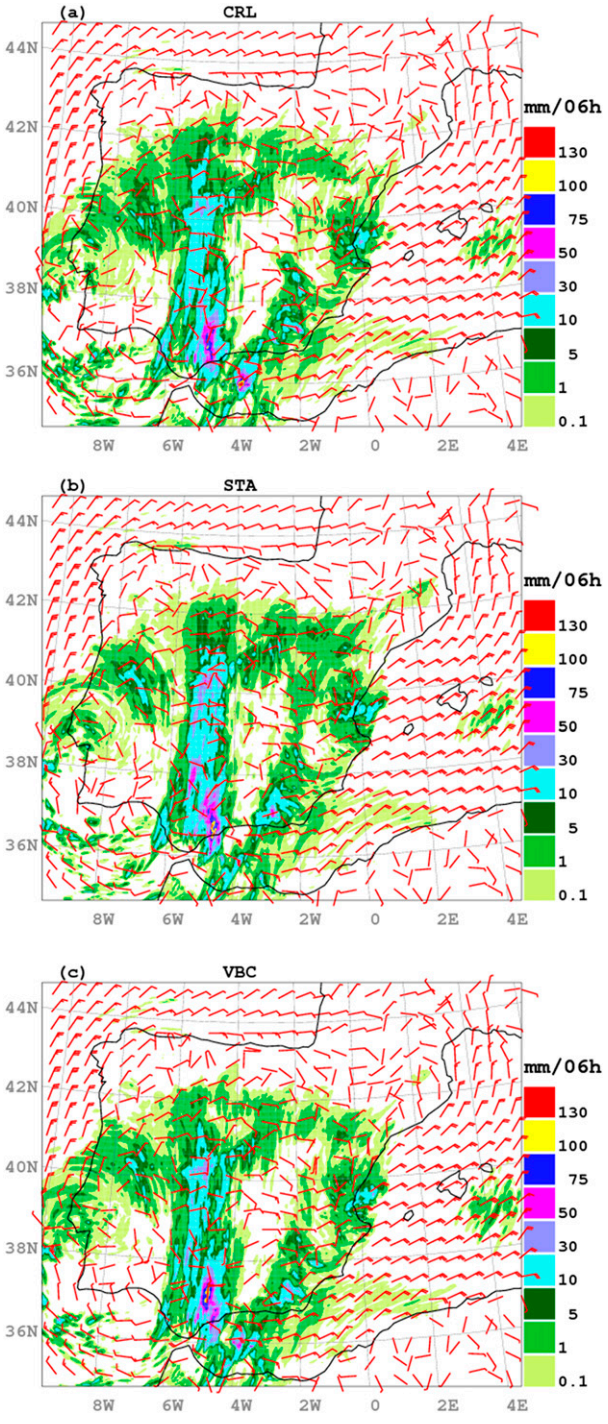

FIG. 12. Simulations of first-six-hour precipitation forecasts [mm $(6\,h)^{-1}$] for (a) CRL, (b) STA, and (c) VBC valid at 0600 UTC 28 Sep 2012. Wind barbs represent 10-m wind forecasts.

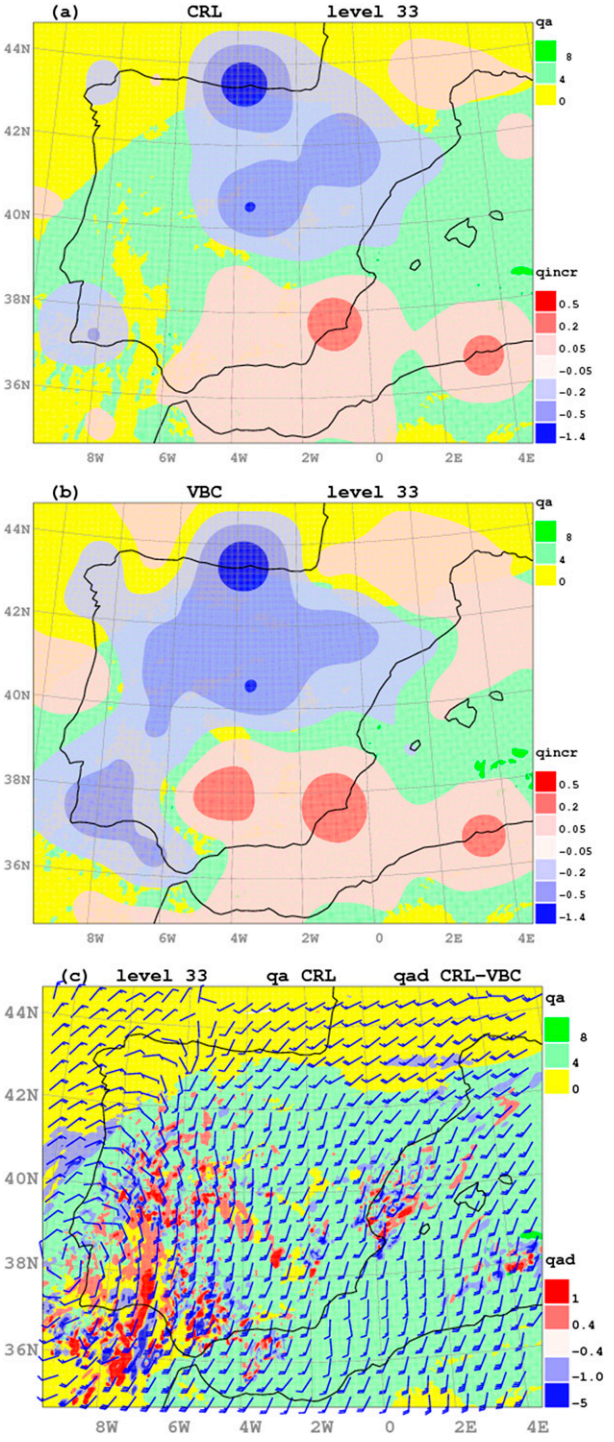

FIG. 13. Analysis increments (qincr) and analysis (qa) of specific humidity ($g\,kg^{-1}$) for the (a) CRL and (b) VBC experiments at model level 33 for 0000 UTC 28 Sep 2012. (c) Simulated specific humidity analysis ($g\,kg^{-1}$) for CRL [identical to the field in (a)], specific humidity analysis differences (qad; $g\,kg^{-1}$) between CRL and VBC, and wind barbs representing wind forecasts for CRL, all at model level 33.

Hungary, Iceland, Ireland, Lithuania, Morocco, Netherlands, Norway, Poland, Portugal, Romania, Slovakia, Slovenia, Spain, Sweden, Tunisia, and Turkey. The constructive comments and suggestions made by three

anonymous reviewers and the editor have led to significant improvements in the manuscript.

REFERENCES

Auligne, T., A. P. McNally, and D. P. Dee, 2007: Adaptive bias correction for satellite data in a numerical weather prediction system. *Quart. J. Roy. Meteor. Soc.*, **133**, 631–642, doi:10.1002/qj.56.

Benjamin, S. G., B. D. Jamison, W. R. Moninger, S. R. Sahm, B. E. Schwartz, and T. Schlatter, 2010: Relative short-range forecast impact from aircraft, profiler, radiosonde, VAD, GPS-PW, METAR, and Mesonet observations via the RUC hourly assimilation cycle. *Mon. Wea. Rev.*, **138**, 1319–1343, doi:10.1175/2009MWR3097.1.

Bennitt, G. V., and A. Jupp, 2012: Operational assimilation of GPS zenith total delay observations into the Met Office numerical weather prediction models. *Mon. Wea. Rev.*, **140**, 2706–2719, doi:10.1175/MWR-D-11-00156.1.

Berre, L., 2000: Estimation of synoptic and mesoscale forecast error covariances in a limited-area model. *Mon. Wea. Rev.*, **128**, 644–667, doi:10.1175/1520-0493(2000)128<0644:EOSAMF>2.0.CO;2.

Bevis, M., S. Businger, T. A. Herring, C. Rocken, R. A. Anthes, and R. H. Ware, 1992: GPS meteorology: Remote sensing of atmospheric water vapor using the global positioning system. *J. Geophys. Res.*, **97**, 15 787–15 801, doi:10.1029/92JD01517.

——, ——, S. Chiswell, T. A. Herring, R. Anthes, C. Rocken, and R. H. Wares, 1994: GPS meteorology: Mapping zenith wet delay on the precipitable water. *J. Appl. Meteor.*, **33**, 379–386, doi:10.1175/1520-0450(1994)033<0379:GMMZWD>2.0.CO;2.

Boniface, K., and Coauthors, 2009: Impact of high-resolution data assimilation of GPS zenith delay on Mediterranean heavy rainfall forecasting. *Ann. Geophys.*, **27**, 2739–2753, doi:10.5194/angeo-27-2739-2009.

Bosilovich, M. G., and Coauthors, 2012: Report of the 4th World Climate Research Programme International Conference on Reanalyses. WCRP Rep. 12/2012, 41 pp. [Available online at http://www.wcrp-climate.org/documents/ICR4_Report.pdf.]

Cucurull, L., J. Vila, and A. Rius, 2002: Zenith total delay study of a mesoscale convective system: GPS observations and fine scale modelling. *Tellus*, **54A**, 138–147, doi:10.1034/j.1600-0870.2002.01252.x.

——, F. Vandenberghe, D. Barker, E. Vilaclara, and A. Rius, 2004: Three-dimensional variational data assimilation of ground-based GPS ZTD and meteorological observations during the 14 December 2001 storm event over the western Mediterranean Sea. *Mon. Wea. Rev.*, **132**, 749–763, doi:10.1175/1520-0493(2004)132<0749:TVDAOG>2.0.CO;2.

Cuxart, J., P. Bougeault, and J.-L. Redelsperger, 2000: A turbulent scheme allowing for mesoscale and large-eddy simulations. *Quart. J. Roy. Meteor. Soc.*, **126**, 1–30, doi:10.1002/qj.49712656202.

Dach, R., U. Hugentobler, P. Fridez, and M. Meindl, 2007: Bernese GPS software version 5.0. Astronomical Institute, University of Bern, Switzerland.

Dee, D., 2005: Bias and data assimilation. *Quart. J. Roy. Meteor. Soc.*, **131**, 3323–3343, doi:10.1256/qj.05.137.

——, and S. Uppala, 2009: Variational bias correction of satellite radiance data in the ERA-Interim reanalysis. *Quart. J. Roy. Meteor. Soc.*, **135**, 1830–1841, doi:10.1002/qj.493.

de Haan, S., 2013: Assimilation of GNSS-ZTD and radar radial velocity for the benefit of very short range regional weather forecasts. *Quart. J. Roy. Meteor. Soc.*, **139**, 2097–2107, doi:10.1002/qj.2087.

De Pondeca, M. S. F. V. D., and X. Zou, 2001: A case study of the variational assimilation of GPS zenith delay observations into a mesoscale model. *J. Appl. Meteor.*, **40**, 1559–1576, doi:10.1175/1520-0450(2001)040<1559:ACSOTV>2.0.CO;2.

Derber, J., and F. Bouttier, 1999: A reformulation of the background error covariance in the ECMWF global data assimilation system. *Tellus*, **51A**, 195–221, doi:10.1034/j.1600-0870.1999.t01-2-00003.x.

Desroziers, G., L. Berre, B. Chapnik, and P. Poli, 2005: Diagnosis of observation, background and analysis error statistics in observation space. *Quart. J. Roy. Meteor. Soc.*, **131**, 3385–3396, doi:10.1256/qj.05.108.

——, ——, ——, and ——, 2012: Assimilation of GNSS ZTD and radar radial velocity for the benefit of very-short-range regional weather forecasts. *Quart. J. Roy. Meteor. Soc.*, **139**, 2097–2107, doi:10.1002/qj.2087.

Douša, J., 2001a: The impact of ultra-rapid orbits on precipitable water vapor estimation using ground GPS network. *Phys. Chem. Earth*, **26**, 393–398, doi:10.1016/S1464-1895(01)00072-2.

——, 2001b: Towards an operational near-real time precipitable water vapor estimation. *Phys. Chem. Earth*, **26**, 189–194, doi:10.1016/S1464-1895(01)00045-X.

——, and G. V. Bennitt, 2013: Estimation and evaluation of hourly updated global GPS zenith total delays over ten months. *GPS Solutions*, **17**, 453–464, doi:10.1007/s10291-012-0291-7.

Eresmaa, R., and H. Järvinen, 2005: Estimation of spatial global positioning system zenith delay observation error covariance. *Tellus*, **57A**, 194–203, doi:10.1111/j.1600-0870.2005.00096.x.

Fabry, F., and J. Sun, 2010: For how long should what data be assimilated for the mesoscale forecasting of convection and why? Part I: On the propagation of initial condition errors and their implications for data assimilation. *Mon. Wea. Rev.*, **138**, 242–255, doi:10.1175/2009MWR2883.1.

Fischer, C., T. Montmerle, L. Berre, L. Auger, and S. Stefanescu, 2005: An overview of the variational assimilation in the ALADIN/France numerical weather-prediction system. *Quart. J. Roy. Meteor. Soc.*, **131**, 3477–3492, doi:10.1256/qj.05.115.

Fouquart, Y., and B. Bonnel, 1980: Computation of solar heating of the earth's atmosphere: A new parameterization. *Beitr. Phys. Atmos.*, **53**, 35–62.

Gendt, G., C. Reigber, and D. Dick, 2001: Near real-time water vapor estimation in a German GPS network—First results from the ground program of the HGF GASP project. *Phys. Chem. Earth*, **26**, 413–416, doi:10.1016/S1464-1895(01)00075-8.

Giard, D., and E. Bazile, 2000: Implementation of a new assimilation scheme for soil and surface variables in a global NWP model. *Mon. Wea. Rev.*, **128**, 997–1015, doi:10.1175/1520-0493(2000)128<0997:IOANAS>2.0.CO;2.

Järvinen, H., E. Andersson, and F. Bouttier, 1999: Variational assimilation of time sequences of surface observations with serially correlated errors. *Tellus*, **51A**, 469–488, doi:10.1034/j.1600-0870.1999.t01-4-00002.x.

Kleijer, F., 2001: Mapping function induced bias in tropospheric delay estimation using GPS. *Phys. Chem. Earth*, **26A**, 467–470, doi:10.1016/S1464-1895(01)00085-0.

Lin, C.-L., T. Chai, and J. Sun, 2000: Adjoint retrieval of wind and temperature fields from a simulated convective boundary layer. *Proc. 14th Symp. on Boundary Layer and Turbulence*, Aspen, CO, Amer. Meteor. Soc., 106–107.

Liu, Z. Q., and F. Rabier, 2002: The interactions between model resolution, observation resolution and observation density in data assimilation: A one-dimensional study. *Quart. J. Roy. Meteor. Soc.*, **128**, 1367–1386, doi:10.1256/003590002320373337.

Lorenz, E., 1965: A study of the predictability of a 28-variable atmospheric model. *Tellus*, **17**, 321–333, doi:10.1111/j.2153-3490.1965.tb01424.x.

Macpherson, S., G. Deblonde, J. Aparicio, and B. Casati, 2008: Impact of NOAA ground-based GPS observations on the Canadian regional analysis and forecast system. *Mon. Wea. Rev.*, **136**, 2727–2746, doi:10.1175/2007MWR2263.1.

Mahfouf, J.-F., K. Bergaoui, C. Draper, F. Bouyssel, F. Taillefer, and L. Taseva, 2009: A comparison of two off-line soil analysis schemes for assimilation of screen-level observations. *J. Geophys. Res.*, **114**, D08105, doi:10.1029/2008JD011077.

——, F. Ahmed, P. Moll, and F. Teferle, 2015: Assimilation of zenith total delays in the AROME France convective scale model: A recent assessment. *Tellus*, **67A**, doi:10.3402/tellusa.v67.26106.

Masson, V., and Coauthors, 2013: The SURFEXv7.2 land and ocean surface platform for coupled or offline simulations of earth surface variables and fluxes. *Geosci. Model Dev.*, **6**, 929–960, doi:10.5194/gmd-6-929-2013.

Mlawer, E. J., S. J. Taubman, P. Brown, M. J. Iacono, and S. Clough, 1997: Radiative transfer for inhomogeneous atmospheres: RRTM, a validated correlated-*k* model for the longwave. *J. Geophys. Res.*, **102**, 16 663–16 682, doi:10.1029/97JD00237.

Poli, P., and Coauthors, 2007: Forecast impact studies of zenith total delay data from European near real-time GPS stations in Météo France 4DVAR. *J. Geophys. Res.*, **112**, D06114, doi:10.1029/2006JD007430.

Rooy, W. C., and P. A. Siebesma, 2010: Analytical expressions for entrainment and detrainment in cumulus convection. *Quart. J. Roy. Meteor. Soc.*, **136**, 1216–1227, doi:10.1002/qj.640.

Sánchez-Arriola, J., and B. Navascués, 2007: Report on surface moisture impact study. EU-FP5 TOUGH Project Deliverable 31, 16 pp. [Available online at http://tough.dmi.dk/deliverables/d31-rh2-impact.pdf.]

——, ——, and J. A. García-Moya, 2006: Report on INM assimilation results. EU-FP5 TOUGH Project Deliverables 46 and 32, 17 pp. [Available online at http://tough.dmi.dk/deliverables/d46-impact-inm.pdf.]

Seity, Y., P. Brousseau, S. Malardel, G. Hello, P. Benard, F. Bouttier, C. Lac, and V. Masson, 2011: The AROME-France convective-scale operational model. *Mon. Wea. Rev.*, **139**, 976–991, doi:10.1175/2010MWR3425.1.

Shoji, Y., M. Kunii, and K. Saito, 2011: Mesoscale data assimilation of Myanmar cyclone Nargis. Part II: Assimilation of GPS-derived precipitable water vapor. *J. Meteor. Soc. Japan*, **89**, 67–88, doi:10.2151/jmsj.2011-105.

Stewart, L., S. Dance, and N. K. Nichols, 2013: Data assimilation with correlated observation errors: Experiments with a 1-D shallow water model. *Tellus*, **65A**, 19546, doi:10.3402/tellusa.v65i0.19546.

Stoew, B., 2004: Description and analysis of data and errors in GPS meteorology. Ph.D. thesis, Chalmers University of Technology.

Vedel, H., and X.-Y. Huang, 2004: Impact of ground based GPS data on numerical weather prediction. *J. Meteor. Soc. Japan*, **82**, 459–472, doi:10.2151/jmsj.2004.459.

——, K. S. Mogensen, and X.-Y. Huang, 2001: Calculation of zenith delays from meteorological data comparison of NWP model, radiosonde and GPS delays. *Phys. Chem. Earth*, **26**, 497–502, doi:10.1016/S1464-1895(01)00091-6.

Webb, F. H., and J. F. Zumberge, 1993: An introduction to GIPSY/OASIS-II. Jet Propulsion Laboratory Publ. D-11088, 300 pp.

Yan, X., V. Ducrocq, G. Jaubert, P. Brousseau, P. Poli, C. Champollion, C. Flamant, and K. Boniface, 2009a: The benefit of GPS zenith delay assimilation to high-resolution quantitative precipitation forecasts: A case-study from COPS IOP 9. *Quart. J. Roy. Meteor. Soc.*, **135**, 1788–1800, doi:10.1002/qj.508.

——, ——, P. Poli, M. Hakam, G. Jaubert, and A. Walpersdorf, 2009b: Impact of GPS zenith delay assimilation on convective-scale prediction of Mediterranean heavy rainfall. *J. Geophys. Res.*, **114**, D03104, doi:10.1029/2008JD011036.